

Energy regenerative damping in variable impedance actuators for long-term robotic deployment

Fan Wu and Matthew Howard^{*†}

Abstract—Energy efficiency is a crucial issue towards long-term deployment of compliant robots in the real world. In the context of variable impedance actuators (VIAs), the main focus has been on improving energy efficiency through reduction of energy consumption. However, the *harvesting* of dissipated energy in such systems remains under-explored. This study proposes a novel variable damping module design enabling energy regeneration in VIAs by exploiting the regenerative braking effect of DC motors. The proposed damping module uses four switches to combine *regenerative* and *dynamic* braking, in a hybrid approach that enables energy regeneration without reduction in the range of damping achievable. A physical implementation on a simple VIA mechanism is presented in which the regenerative properties of the proposed module are characterised and compared against theoretical predictions. To investigate the role of variable regenerative damping in terms of energy efficiency of long-term operation, experiments are reported in which the VIA equipped with the proposed damping module performs sequential reaching to a series of stochastic targets. The results indicate that the combination of variable stiffness *and* variable regenerative damping is preferable to achieve the optimal trade-off between task performance and energy efficiency. Use of the latter results in a 25% performance improvement on overall performance metrics (incorporating reaching accuracy, settling time, energy consumption and regeneration), over comparable schemes where either stiffness or damping are fixed.

I. INTRODUCTION

The mass deployment of robotic solutions in manufacturing causes huge energy demand. For example, 8% of the total electrical energy usage in production processes of automotive industries is consumed by industrial robots [1]. For ecological and economic reasons, this motivates research on reducing the energy cost of industrial robots. Furthermore, with the extensive deployment of compliant robots expected in the near-future for human-robot collaboration, medical and civil services, *etc.*, this imperative to save energy is likely to become even more critical. Variable impedance actuators (VIAs) are believed to be the key for the next generation of robots to interact safely with uncertain environments and provide better performance in cyclic tasks and dynamical movements [2]. For example, the physical compliance incorporated in *variable stiffness actuators* (VSAs) (*e.g.*, using elastic components such as springs) enables energy storage, which can be used to (i) absorb external energy introduced into the system (*e.g.*, from collisions) to enhance safety, and (ii) amplify output power by releasing stored energy as and when required by the task [3].

Recently, much research effort has gone into the design of *variable physical damping* actuation, based on different

principles of damping force generation (see [4] for a review). Variable physical damping has proven to be necessary to achieve better task performance, for example, in eliminating undesired oscillations caused by the elastic elements of VSAs [5], [6]. It is also demonstrated in [5] that variable physical damping plays an important role in terms of energy efficiency for actuators that are required to operate at different frequencies, to optimally exploit the natural dynamics. However, while these studies represent important advances in terms of improving the efficiency of *energy consumption* in VIAs, the importance of variable physical damping may be underestimated, because the potential to *harvest energy dissipated by damping* has so far received little attention.

To address this, this paper extends the variable damping technique introduced by [7] to take into account the energy regeneration capabilities of DC motors. In contrast to prior approaches, a circuit design using four switches—considering the fact that the rotation of a revolute robot joint is bidirectional while typical power sources for energy storage are unidirectional—is introduced that enables adjustment of the electrical damping effect, while increasing the damping range available to the controller [8]. The relation of the damping effect and the power of regeneration of the proposed damping module is investigated, and shows a non-monotonic relation emerges that requires balancing a trade-off between damping allocation and energy regeneration in a non-trivial way. Furthermore, evaluations in terms of a stochastic movement task of a physical VIA mimicking long term industrial operation, demonstrate that variable regenerative damping, *in combination with an optimally exploited variable stiffness mechanism*, can contribute both enhanced dynamic performance and improved energy efficiency (in terms of both consumption and regeneration). Measuring performance through four metrics (accuracy, settling time, energy consumption and regeneration), results reported here indicate that this approach can outperform schemes where stiffness and/or damping are fixed by up to 25.03% overall.

II. BACKGROUND

The problem of energy efficiency in compliant robotic systems has been addressed via different approaches from the perspectives of control or design, which can be mainly categorised into studies that (i) look at *exploiting energy storage* in periodic or discrete movements, or (ii) focus on *reducing energy consumption* via the mechanical design. In the following subsections, the basic concept of power flow of VIAs is introduced, followed by an account of the theory of regenerative braking of electric motors. Against this backdrop, a summary of related work on the topic of energy efficiency for such systems is provided in §III.

^{*}Fan Wu and Matthew Howard are with the Centre for Robotics Research, Department of Informatics, King's College London, UK {fan.wu, matthew.j.howard}@kcl.ac.uk.

[†]This work was supported in part by the UK Engineering and Physical Sciences Research Council (EPSRC) SoftSkills project, EP/P010202/1.

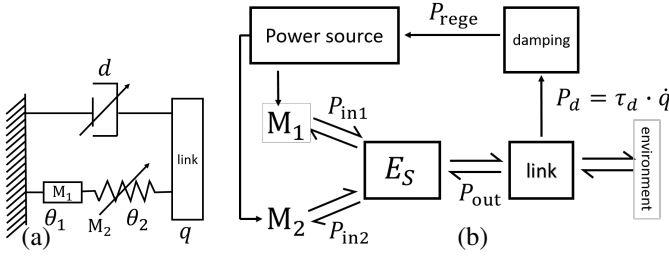


Fig. 1: Schematic diagrams of (a) a VIA represented by a mass-spring-damper model, and (b) the corresponding power flow. The arrow between damping module and power source shows that the energy dissipated via damping can be harvested and used to recharge the power source.

A. Power flow of VIAs

The type of VIA considered in this paper can be represented by the mass-spring-damper model depicted in Fig. 1(a). The link, whose position is denoted by q , is connected in series to a motor and a variable spring. The equilibrium position is controlled by the motor M_1 and the stiffness is modulated by another motor M_2 . The damper in this system is arranged between the link and the base, and the damping d is independently controllable.

The corresponding power flow of this actuation system is shown in Fig. 1(b). A power source is assumed to be used to power the motors M_1, M_2 . The elastic element, *i.e.*, the spring in the mass-spring-damper model, can be viewed as an energy tank in the actuator that stores potential energy E_s . In general, the power flow of this element can be represented in the form of power conversation: $P_{in} = P_{out} + \dot{E}_s$. More specifically,

$$\begin{aligned} \dot{E}_s &= \frac{\partial E_s}{\partial q} \dot{q} + \frac{\partial E_s}{\partial \theta_1} \dot{\theta}_1 + \frac{\partial E_s}{\partial \theta_2} \dot{\theta}_2 \\ &= -\tau_s \dot{q} - \tau_{s1} \dot{\theta}_1 - \tau_{s2} \dot{\theta}_2 \\ &= -P_{out} + \underbrace{P_{in1} + P_{in2}}_{P_{in}} \end{aligned} \quad (1)$$

where P_{in}, P_{out} is the power drained and delivered by the compliant actuation module, respectively, and \dot{E}_s is the rate of change¹ of the energy stored in the elastic elements. P_{in} consists of power input from both motors (P_{in1} and P_{in2}). As shown in the diagram, P_{out} is bi-directional which means that the elastic element can deliver energy to or receive energy from the link. The link can output the energy to or receive energy from the environment via interaction. The spring stores energy when $P_{in} > P_{out}$. When it releases energy such that $\dot{E}_s < 0$, it can contribute to positive output power P_{out} while decreasing the required power P_{in} from motors. It can be seen that regulating the energy flow around the elastic element is one of the keys to improving the energy efficiency of VSAs. Actually, much research effort has been devoted in this direction, dating back to early research in robotic locomotion and passive-dynamic walking, such as the energy efficient walking robots developed by Collins [9] that utilised compliant ankles (further examples are discussed in §III). Note that, focusing on this part of the energy flow essentially aims to improve efficiency in terms of *energy consumption*.

An alternative to this is to focus on improving efficiency through *energy regeneration*. From Fig. 1(b), it can be seen

that the link dissipates energy via damping elements, a uni-directional flow. If the latter primarily consist of frictional elements, this energy is wasted. However, if the damping mechanism is such that the dissipated energy can be harvested, this energy has the potential to be used to recharge the power source and decrease the overall net consumption. So far, this possibility has received little attention and motivates the present research into the design of damping modules that can realise such regeneration.

B. Dynamic and regenerative braking

Among the different methods of implementing variable physical damping in the literature, the approach of *damping by motor braking* presents the greatest promise for incorporating energy harvesting by utilising the regenerative braking technique. Regenerative braking technology has been widely used in vehicles driven by electric motors [10] or equipped with regenerative suspension systems [11]. In the context of robotics, two main approaches have been proposed that enable variable damping through the use of DC motors, namely (i) *dynamic braking* and (ii) *regenerative braking*. In both cases, the back electromotive force is used to resist movement proportional to the effective resistance of the damper motor circuit, causing a variable damping effect. The following briefly outlines these schemes.

Scheme 1 - Dynamic braking: Dynamic braking in the context of VIA design was first proposed by [7]. A circuit diagram for this scheme is illustrated in Fig. 2(a). In this mode, the damping effect is modulated by changing the duty-cycle D_d that controls the portion of time that a switch S_1 spends in the open or closed position, thereby altering the effective resistance of the circuit. The damping coefficient follows the equation

$$d = \frac{n_d^2 k_t^2 D_d}{R_m} = \bar{d}_1 D_d \quad (2)$$

where n_d is the gear ratio of damping motor, k_t is the torque constant and R_m is the resistance of the motor. Note that, since $0 \leq D_d \leq 1$, the maximum damping coefficient that can be provided by dynamic braking is $\bar{d}_1 = n_d^2 k_t^2 / R_m$.

In energy terms, dynamic braking is effective since it dissipates kinetic energy of the output link as heat in the electrical circuit. It does not, however, charge energy to any electrical source, so the regeneration power is zero ($P_{rege} = 0$). In other words, this (potentially useful) energy is simply discarded, reducing the overall energy efficiency of the system.

Scheme 2 - Regenerative braking: Regenerative braking refers to the situation where the power generated by the motor through kinetic motion of the output link is used to recharge an electrical storage element (*e.g.*, battery, supercapacitor). To implement regenerative braking, the electrical storage element can be simply connected to the circuit of the damping motor, as shown in [12]. In the context of VIA design, this can be implemented through the circuit in Fig. 2(b).

In regenerative braking mode, the damping effect is dependent on the combined effective resistance of the circuit containing the electrical storage element. Similar to dynamic braking, this can be modulated by controlling the duty-cycle D_r of a switch. The damping coefficient and the regeneration

¹Throughout this paper \dot{a} denotes the time derivative of the quantity a .

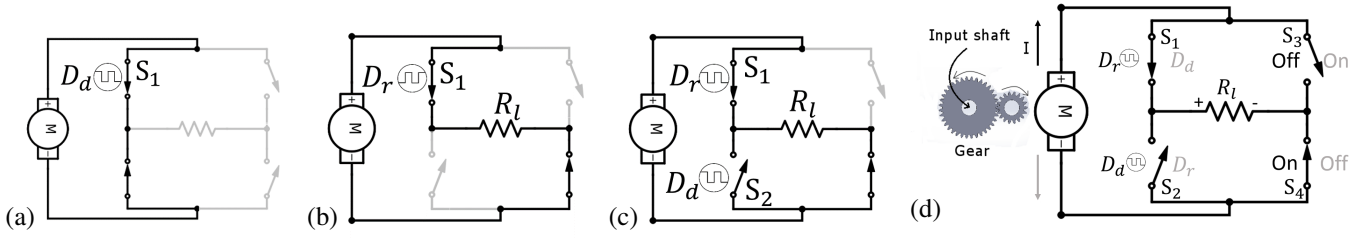


Fig. 2: Conceptual diagrams of (a) dynamic, (b) regenerative, (c) hybrid dynamic-regenerative, and (d) bidirectional hybrid dynamic-regenerative braking circuits.

power can be calculated as

$$d = \frac{n_d^2 k_t^2 D_r}{R_m + R_l} = \bar{d}_2 D_r \quad (3)$$

$$P_{\text{rege}} = \frac{R_l n_d^2 k_b^2 \dot{q}^2 D_r}{(R_m + R_l)^2} = \alpha \bar{d}_2 \dot{q}^2 D_r, \quad (4)$$

respectively, where R_l is the resistance of the electrical source and $\alpha = R_l/(R_m + R_l)$. k_b is the back-EMF constant and is equal to k_t .

Note that, introducing regenerative braking means that the mechanical energy that is otherwise discarded in the dynamic braking scheme can be harvested, enhancing the overall energy efficiency of the system. However, note also that, compared to dynamic braking, the maximum damping coefficient that can be produced by regenerative braking, $\bar{d}_2 = n_d^2 k_t^2 / (R_m + R_l)$, is *decreased* since adding an electrical load for charging increases the total equivalent resistance of the circuit. This can be a drawback in applications where higher levels of damping are needed (*e.g.*, when there is need for a high dynamic response and therefore heavy braking of rapid movements). Another issue is that, since the electrical storage element is usually unidirectional, the current in Scheme 2 has to be unidirectional as well. In order to deal with current following in both directions resulted from the bidirectional movements (which is common in robotic applications), a reversing mechanism is needed. One solution for this is to introduce another switch, as illustrated in Fig. 2(d)—this will be introduced in detail in §IV.

III. RELATED WORK

Over the last decade or more, a number of studies has been conducted in the area of energy efficient robotic actuation. The following is a review of this work, set in the context of the theoretical considerations introduced in §II.

A. Exploiting energy storage

As discussed above (§II-A), the energy storage capability introduced by the elastic elements of VIAs brings not only the advantage of impact tolerance, but also the possibility of improving energy efficiency by reusing the stored energy. As shown in Fig. 1(b), the power flow between the elastic element and output link is bidirectional, which means that energy can be stored in the elastic element, *e.g.*, by absorbing impact energy during interaction with the environment. It can also build up the potential energy by receiving the power from motors and then releasing at the best timing to amplify the output power. The idea of exploiting natural dynamics of physical compliance has been utilised in several lines of

research considering problems of periodic movements such as walking robots [13], [14], [15], [16], lower limb prosthetics [17], cyclic manipulations [18], [19], [20], [21], [22], and discrete movements like throwing [23], [24]. While the use of springy legs has a long history and seminal work can be dated back to the 1980s [25], Collins [9] was the first to successfully demonstrate human-level efficiency on a passive-dynamic walker. One of the keys to its success was the implementation of compliant ankles based on findings from biomechanics about human walking. Vanderborght [14], [15] proposed to exploit the natural dynamics by fitting the compliance of the actuator to the natural compliance of the desired trajectory. The principle is followed by recent development of robotic locomotion driven by compliant actuators [16]. However, new challenges, such as dynamic environments, uncertainties and the complexity of tasks facing robots running in the real world require more advanced tools like optimisation-based numerical solutions to seek energy efficient control.

For cyclic manipulation, [21] used resonance-based control to find the energy optimal constant stiffness for a pick-and-place task. Time-varying optimal stiffness modulation can be solved by optimal control approaches, as demonstrated in [26], [20]. However, the solvable optimal control formulation requires that the periodicity of movements holds perfectly. For a specific problem, *e.g.*, ball dribbling, [22] developed a controller to dribble a ball stably using minimal peak power based on analysis of the stability of dribbling limit cycles and the effects of hand stiffness for robustness and energy efficiency.

The aforementioned optimal control approach has also been used to find the energy-optimal trajectory for explosive movements like throwing [23]. Such kind of problems can be formulated as maximising the output link velocity at the final time [24]. Time-varying optimal stiffness profiles can be solved as a result of optimisation to exploit the power amplification effect as discussed in §II-A. Energy efficiency demand in this case can be viewed as the need to output maximum instantaneous power using limited energy inflow.

B. Reducing energy cost of stiffness modulation

Given the power flow of VIAs (see Fig. 1(b)) it is clear that the power fed into the compliant elements may be taken from both motors. In the early development of series elastic actuators (SEAs) and VSAs it was observed that the adjustment of stiffness causes a lot of energy consumption. Even when $P_{\text{in}2} = 0$, there may still be an electrical cost on the motor in generating force to maintain the elongation or compression of the elastic elements. This drawback motivated several studies investigating designs to minimise the energy consumption of

stiffness modulation via P_{in2} and extra electrical consumption for maintaining stiffness. To name a few, examples are compliant actuators based on a lever mechanism [27] and the minimalistic stiffness modulator proposed by [28], both of which were proposed to avoid having motor drives work against spring forces. Parallel springs are implemented in [29] and [30] to reduce required torque by locking potential energy into the parallel springs.

Indeed, successful exploitation of natural dynamics relies heavily on a suitable mechanical design. The limitation of the above work is that the analysis is based on the decomposition of energy consumption to investigate the cost of stiffness modulation separately. The overall energy cost in the scenarios of dynamic movements is highly task dependent, thus it requires some standardised metrics for different classes of tasks to evaluate the energy efficiency of the compliant actuators.

C. Regenerative braking

The work described in the preceding two sections have shown that the energy efficiency problem has to be addressed by both design and control. Focus has been placed on optimising the power flow of the elastic elements, however, the other major element in the whole power flow relation, *i.e.*, the dissipation $P_d = \tau_d \dot{q}$, has attracted little attention. As noted in §II-B, this dissipated energy need not be lost, instead it can be harvested for later use. The approach taken in this paper, therefore, is to combine the roles of energy harvesting and damping, inspired by the regenerative braking technology used in vehicles.

Energy regeneration can be realised through both the motor drives and variable damping components. As shown in Fig. 1(b), the power flow between motors and the spring can be bidirectional. For example, [31] implemented regenerative electric motor drivers on the MIT Cheetah, relying on the simple fact that electric motors can work as generators². By doing this, the motor is used to both actuate and brake the joint. The same regenerative braking principle is used as a kinetic energy harvester on a lower limb exoskeleton [12] where the motor is purely a generator. The regenerative braking technique is attractive since it can be incorporated with variable damping components which use DC motor damping effects to generate braking force [7].

However, the requirements for the regenerative damping system to be used with VIAs are different from the above use cases. First, for general purpose compliant actuators, the movement is generally bidirectional, but typical electrical energy storage elements (*e.g.*, batteries) are unidirectional, which indicates that a conversion mechanism is needed to ensure that the battery can be charged by energy from both directions of movement. This is different from the case where, in walking and running, the impact power from contact is basically unidirectional. Secondly, regenerating energy dissipated through variable physical damping component is generally coupled with the damping coefficient it provides. Energy regeneration assigns an additional role for variable damping, thus more investigation is needed to determine appropriate control strategies, in order to balance the trade-off between optimality of energy cost/regeneration and task achievement for specific tasks. The next section describes how both issues

can be addressed by (i) proposing a damping module design capable of harvesting energy from bidirectional movements, and (ii) evaluating optimal control as a means for dealing with the energy/task performance trade-off.

IV. HYBRID DYNAMIC-REGENERATIVE BRAKING

To meet the requirements for the regenerative damping system to be used with VIAs, this section presents a variable damping scheme—termed *hybrid braking*—that switches between dynamic braking (Scheme 1 as described in §II-B) and pure regenerative braking (Scheme 2 in §II-B) to achieve the optimal benefits of both.

A. Hybrid damping circuit

The hybrid damping scheme proposed here is implemented through the circuit depicted in Fig. 2(c). It uses two switches (denoted S_i , $i \in \{1, 2\}$) that switch at high frequency between (i) pure regenerative braking, and (ii) a blend of dynamic and regenerative braking. The principle by which the proposed scheme operates is as follows.

When switch S_2 is open, the module acts in regenerative braking mode, whereby current flows through the power storage element, with the effective resistance (damping level) determined by the duty cycle of S_1 . (Note that, this results in an equivalent circuit to that used in Scheme 2, *cf.* Fig. 2(b).) On the other hand, when S_1 and S_2 are closed, there is a short circuit that causes current to bypass the resistive load R_l , creating a dynamic braking effect. In this case, the damping level can be determined by keeping S_1 closed and modulating the duty cycle of S_2 . This enables a third braking scheme to be defined, alongside Schemes 1 and 2, as follows.

Scheme 3 - Hybrid braking: When the required damping d^* is small enough, *i.e.*, $d^* \leq \bar{d}_2$, it can be provided by pure regenerative braking, so S_2 is opened ($D_d = 0$). When the required damping is greater, *i.e.*, $d^* > \bar{d}_2$, S_1 is closed ($D_r = 1$) and D_d is used to control S_2 to blend dynamic and regenerative braking.

The resulting damping coefficient and regeneration power are:

$$d = \bar{d}_2 D_r + \alpha \bar{d}_3 D_d \quad (5)$$

$$P_{\text{rege}} = \alpha \bar{d}_2 \dot{q}^2 (D_r - D_d) = P_{\text{rege}}^0 \dot{q}^2 \quad (6)$$

where $P_{\text{rege}}^0 = \alpha \bar{d}_2 (D_r - D_d)$. Note that, if $D_r = D_d = 1$, the same maximum damping coefficient as that achievable in a pure dynamic braking can be achieved, *i.e.*, $\bar{d}_3 = \bar{d}_1$. This, however, comes at the cost of the regeneration power vanishing ($P_{\text{rege}} = 0$).

B. Hybrid Damping Control Modes

In principle, each of the switches in the proposed circuit may be independently controlled by its own duty-cycle. While this enhances the flexibility of the damping module, it also introduces an undesirable layer of complexity to its control.

²Note that, the Cheetah is not based on physical compliance but active impedance control, so that there is no elastic element between the link and motors that can store potential energy.

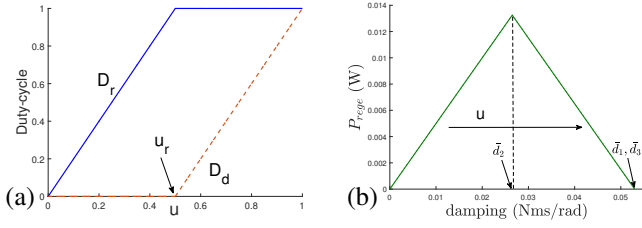


Fig. 3: Hybrid damping control modes. (a) Mapping from control input u to duty cycles D_r, D_d . (b) Relation between regeneration power and damping.

To address this, and enable the simple control of the module through a single control variable $u \in [0, 1]$, the duty cycles of the switches can be coupled through the following relation

$$D_r = \begin{cases} \frac{u}{u_r}, & u \leq u_r \\ 1, & u > u_r \end{cases}$$

$$D_d = \begin{cases} 0, & u \leq u_r \\ \frac{u - u_r}{1 - u_r}, & u > u_r \end{cases} \quad (7)$$

where u_r corresponds to the maximum damping coefficient of regenerative braking ($d(u_r) = \bar{d}_2$) and depends on the user's selection. In this paper, u_r is chosen to be 0.5. Substituting (7) into (5), the damping coefficient as a function of u is simplified to

$$d(u) = \bar{d}_3 u. \quad (8)$$

As illustrated in Fig. 3(a), when $u \leq 0.5$, D_d remains at zero (i.e., switch S_2 is open) and D_r is linearly mapped from $u \in [0, 0.5]$ to $[0, 1]$, while when $u > 0.5$, D_r is held at unity ($D_r = 1$ so S_1 is closed) and D_d is linearly mapped from $u \in [0.5, 1]$ to $[0, 1]$.

The relation between the damping coefficient d and the power regeneration P_{rege} for a fixed angular velocity is shown in Fig. 3(b). As can be seen, the relationship is non-monotonic and there is a peak for P_{rege} when $d = \bar{d}_2$, i.e., at the upper boundary of the pure regenerative braking domain.

C. Bidirectional damping

The hybrid damping circuit described so far enables the modulation of damping force associated with unidirectional motion of the output link. In order to realise damping of bidirectional motion (as is common in many robotic applications), it is necessary to ensure that the current generated by the damping motor always flows into the positive terminal of the electrical storage element. This can be achieved by a four-switch design of the damping circuit, as illustrated in Fig. 2(d). When the current flows from the positive terminal of the damping motor (as shown by the black arrow in Fig. 2(d)), S_3 is open and S_4 is switched on. When the current flows from the negative terminal of the motor (as shown by the grey arrow), S_3 is closed and S_4 is open, and S_1 is controlled by D_d and S_2 is controlled by D_r .

It should be further noted that, this latter circuit, implements the (bidirectional versions of) the two damping schemes outlined in §II-B as special cases. For example, (i) holding S_2, S_3 open, S_4 closed and varying the duty cycle of S_1 results in regenerative braking, while (ii) holding S_3, S_4 open, S_1 closed, and varying the duty cycle of S_2 results in pure dynamic

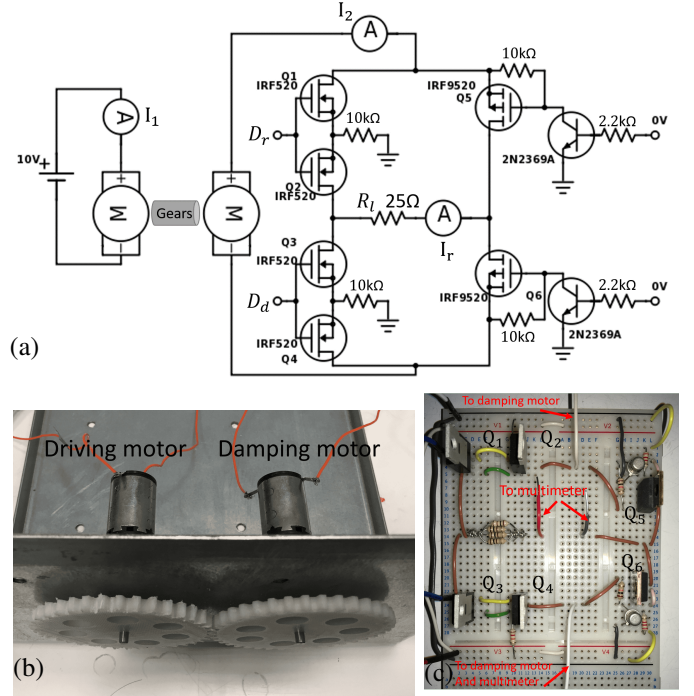


Fig. 4: Damping and power regeneration measurement experiment setup. Shown are (a) circuit diagram of the experiment setup, (b) damping test rig, and (c) damping circuit module.

braking. In other words, the same hardware can be used to realise all three damping schemes. In the following sections, for brevity, the term regenerative damping will be used to refer to the proposed hybrid damping scheme in the context of VIAs.

D. Physical realisation of the damping module

This section presents the physical realisation of the hybrid damping circuit design introduced above and an experiment to verify the theoretical predictions about the damping/regeneration performance trade-off. The experimental set up is shown in Fig. 4. As a simple test-rig, two identical DC motors (Maxon A-max 22/110125) are coupled through a pair of spur gears to enable one motor (driver) to drive the other (damper), see Fig. 4(b). The two motors have the same gearhead with $n_d = 20$. The torque constant is $k_t = 0.0212 \text{ Nm/A}$ and the motor resistance $R_m = 21.2\Omega$.

The damper motor is connected to the circuit depicted in Fig. 4(a), that is the physical realisation of the conceptual diagram Fig. (d). In this circuit design, a pair of N-channel MOSFETs (IRF520) is used as one switch to make sure that the switching mechanism works properly for bidirectional current. In Fig. 4(a), the pair of Q_1, Q_2 works as the switch S_1 , and Q_3, Q_4 make the switch S_2 . Two P-channel MOSFETs (IRF9520) with BJTs (2N2369A) are used as switches S_3, S_4 . The duty-cycles D_r, D_d are controlled by PWM signals from an Arduino Mega2560 board. By setting 0V signals on the control pins for Q_5, Q_6 , they are open for just one current direction but closed for the other. For the ease of power measurement, a resistor is used to represent the electrical load ($R_l = 25.3\Omega$).

In the experiment, the driving motor is used to drive the system while the damping applied by the second motor is

varied, and the resultant motion (motor speeds and energy regeneration) is recorded. Specifically, the driving motor is powered by a 10V DC power supply ($V_{bb} = 10V$) while the damping motor control input u is varied from 0 to 1 in increments of 0.1 (with the corresponding duty-cycles D_r, D_d computed by (7)). Simultaneously, three multimeters (Rapid DMM 318) are used to measure the currents I_1, I_2, I_r through the driving motor, damping motor and the electrical load R_l respectively. The latter data are used to compute the angular speed of the motors ω and the damping torque τ_d according to

$$V_{bb} = I_1 R_m + n_d k_t \omega \quad (9)$$

$$\tau_d = n_d k_t I_2 = d(u) \omega. \quad (10)$$

The damping coefficient $d(u)$ for a given u is then estimated by

$$\hat{d}(u) = \frac{n_d^2 k_t^2 I_2}{V_{bb} - I_1 R_m} \quad (11)$$

and the regeneration power (normalised by the square of speed for comparison) is estimated as

$$\hat{P}_{\text{rege}}^0 = \frac{n_d^2 k_t^2 I_r^2 R_l}{(V_{bb} - I_1 R_m)^2}. \quad (12)$$

The results based on the data collected from 10 repetitions of the experiment is plotted in Fig. 5 alongside the theoretical predictions (from §IV-B).

It can be seen that, the experimental data (blue lines in Fig. 5) is in good agreement with the model predictions (red lines in Fig. 5). By increasing u from 0 to 1, the damping coefficient d increases almost proportionally. Furthermore, it is verified that, when fixing the angular speed (P_{rege} has been normalised to estimate P_{rege}^0), the relation between P_{rege}^0 and u is non-monotonic with a peak found at $u = 0.5$. However, the experimental data indicates that for both regions ($u \in [0, 0.5]$ and $u \in [0.5, 1]$), the regeneration coefficient is not linearly dependent on the control input. This modelling error might be due to unmodelled effects such as circuit inductance and switching frequency.

V. SIMULATION AND EVALUATION WITH IDEAL VIA

Having verified the feasibility of physically implementing the proposed damping module, it is necessary to evaluate its use in the context of robot control. As noted in §III-C, the dual role of the damping module, both for braking and energy harvesting introduces a trade-off between task performance and energy efficiency. To resolve this, it is proposed to employ optimal control to determine the best damping modulation strategy according to task demands. This section presents an evaluation of such a scheme to control the hybrid braking module in the context of a simple example task of target reaching.

For this, a model of a simple pendulum, subject to viscous friction and actuated by an ideal VIA is used

$$ml^2 \ddot{q} + b\dot{q} = k(u_2)(u_1 - q) - d(u_3). \quad (13)$$

Here, for simplicity, $m = 1\text{kg}$, $l = 1\text{m}$, $b = 0.01\text{Nms/rad}$. The motor positions θ_1, θ_2 are assumed to be directly controlled by control inputs u_1, u_2 . u_3 is the control input for damping d . The right hand side of (13) is the joint torque applied by the ideal VIA, $u_1 \in [-\pi/2, \pi/2]$ rad controls the

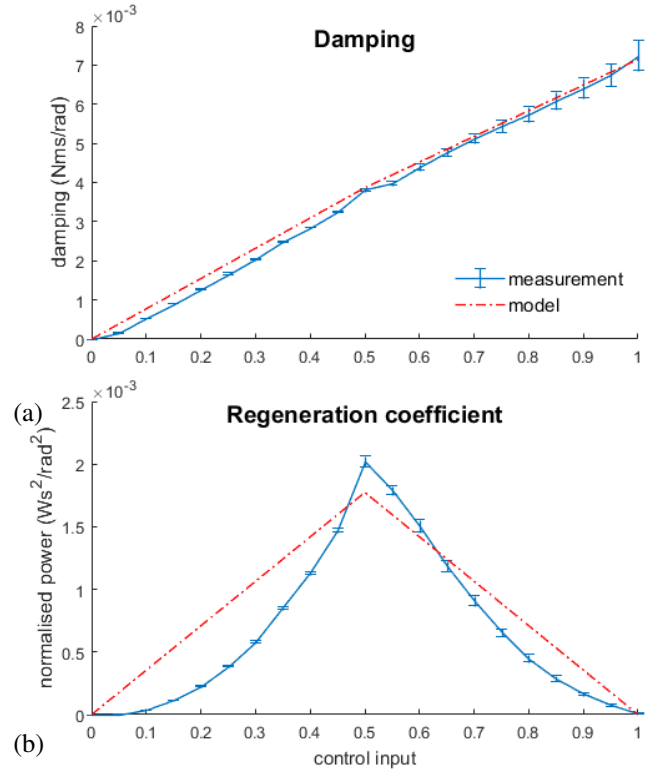


Fig. 5: Results of the damping test experiment. The (a) damping coefficient, and (b) regeneration coefficient for each tested control input $u \in [0, 1]$ are shown. The blue error bars represent the means and standard deviations of data points for 10 repetitions of the experiment and the red line shows the values predicted by the model.

equilibrium position and the stiffness $k(u_2)$ is proportional to the control input $u_2 \in [0, 1]$, i.e.,

$$k(u_2) = \bar{k} u_2 \quad (14)$$

where $\bar{k} = 200\text{Nm/rad}$ is the maximum stiffness. The damping $d(u_3)$ as a function of u_3 is given by (8). The corresponding power of regeneration P_{rege} is assumed to be computed by the model introduced in §IV. The parameters³ that characterise the variable damping module are selected to be $\bar{d}_3 = 50\text{Nms/rad}$, $\bar{d}_2 = 25\text{Nms/rad}$ and $\alpha = 0.5$. The control frequency is set to 50Hz.

The task is to reach a target $q^* = \pi/3\text{rad}$ from the initial position $q = 0\text{rad}$ within a finite time t_f as quickly and accurately as possible, while minimising the energy consumption and control effort. This can be described through minimisation of the cost function

$$J = \int_0^{t_f} [w_1(q(t) - q^*)^2 + w_2(u_1(t) - q^*)^2 + w_3 u_2^2(t) - w_4 P_{\text{rege}}] dt \quad (15)$$

where $w_1 = 1000$, $w_2 = w_3 = 1$, $w_4 = 0.01$ are weighting parameters. These parameters are selected to take account of the different scales of the terms and allow reaching within a

³These parameters are arbitrarily chosen to give response within a second. Experimentation shows the result is not sensitive to these values.

second.

To simplify the analysis, in the below, the command for equilibrium position is fixed at $u_1 = \pi/3$, while the commands for stiffness and damping are allowed to vary. The optimal open-loop control sequence for the latter is computed through the Iterative Linear Quadratic Regulator (ILQR) method [32] with the proposed hybrid braking scheme, and the resultant trajectory of the system is computed by simulating the execution of the open-loop command using the 4th Order Runge-Kutta method.

To evaluate the energy efficiency of the proposed approach, the total mechanical work⁴ and the total regenerated energy are computed from the resultant trajectories, *i.e.*,

$$E = \int_0^{t_f} k(u_1 - q)\dot{q} dt \quad (16)$$

$$E_{\text{rege}} = \int_0^{t_f} P_{\text{rege}}(t) dt, \quad (17)$$

respectively. The net energy cost can be defined as

$$E_{\text{net}} = E - E_{\text{rege}}. \quad (18)$$

The percentage ratio of energy regeneration⁵ can be computed by

$$\eta = \frac{E_{\text{rege}}}{E}. \quad (19)$$

For comparison, the experiment is repeated with (i) pure dynamic braking (Scheme 1), (ii) pure regenerative braking (Scheme 2), (iii) the case where the damping is fixed at the maximum power of regeneration ($d = \bar{d}_2$), and (iv) a critically damped system. In the latter, the stiffness is chosen to be $k = 100\text{Nm/rad}$ and the damping is fixed to $d = 20\text{Nms/rad}$ such that the damping ratio $\zeta = d/2\sqrt{km} = 1$.

The results are illustrated in Fig. 6. As can be seen, the trajectory of the critically damped system reaches the target slowly but without overshoot (Fig. 6(a)). The system with fixed damping reaches the target quicker than the critically damped one, because it can exploit the variable stiffness. The system with regenerative braking reaches the target quicker still, however, since the damping range is limited in this case, it suffers from overshoot once it reaches the target. In contrast, the dynamic braking and hybrid braking systems reach the target quickest without overshoot, so perform best in terms of accuracy.

Looking at Fig. 6(c), however, it can be observed that the dynamic braking performs worst in terms of net energy cost, since no energy is recovered throughout the movement. This contrasts with the hybrid approach, that achieves fast and accurate movement while also achieving 27.4% energy recovery, thereby lowering the net energy cost.

Overall, the proposed hybrid scheme offers a good trade-off between task accuracy and energy efficiency.

VI. EXPERIMENT: LONG-TERM ROBOTIC DEPLOYMENT

In the real-world deployment of compliant robotic systems, VIAs must be able to withstand many use cycles with un-

⁴As motors are not explicitly involved in the model, the mechanical work computed here corresponds with the integration of the power delivered onto the plant (P_{out} in Fig. (b)), not the power from motors side (P_{in}).

⁵Note that, for simplicity, it is assumed here that there is 100% kinetic to electric energy transmission efficiency of the DC motor. In practice, losses are likely to occur due to friction and losses in the conversion from the mechanical to the electrical domain.

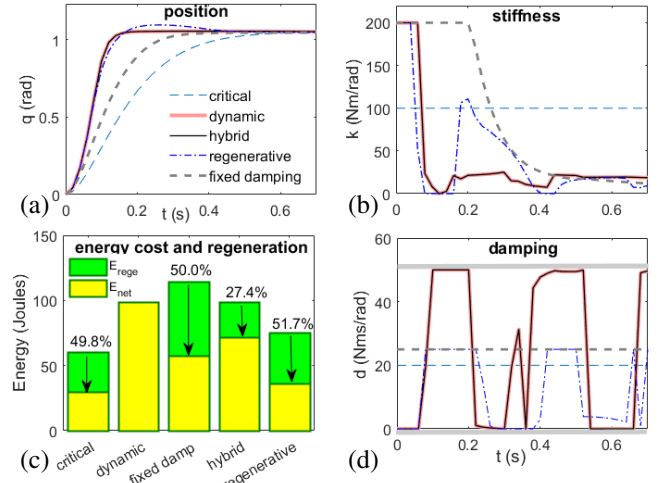


Fig. 6: Test of reaching task on simple pendulum with ideal VIA. Shown are optimal (a) joint angular trajectories, (b) stiffness, and (c) total mechanical work and percentage ratio of energy regeneration for different damping schemes, and (d) damping profiles.

predictable task demands. This section reports an experiment designed to evaluate the likely effectiveness of the proposed damping scheme in the context of long-term use. For simplicity, the test case chosen is the task of performing consecutive point-to-point reaching movements to a series of random targets generated on the fly (*i.e.*, as the robot is moving). Note that, while such tasks are common in many robotic applications (*e.g.*, a robot deployed to tidy a room may have to reach and grasp many objects at uncertain locations), they are challenging from the point of view of energy management, since the movements are non-periodic and unpredictable, hence, physical factors, such as the natural frequency of the device cannot easily be exploited. The following reports the experimental design and procedure in detail.

A. Hardware specifications

To evaluate its use, the damping module developed in §IV-D is implemented on a physical VIA. Specifically, the experimental platform consists of a 3D-printed, single-joint robot using the Mechanically Adjustable Compliance and Controllable Equilibrium Position Actuator with Variable Damping (MACCEPA-VD) [7], [33] mechanism for actuation (see Fig. 7(b)). A schematic diagram of the system is shown in Fig. 7(a) alongside the design parameters. In this implementation of the MACCEPA-VD, the equilibrium position and joint stiffness are controlled by two servomotors (Hitec HS-7950TH and Hitec HSR-5990TG, respectively). A DC motor (Maxon A-max 22/110125) is attached to the joint to serve as the damping motor, whose damping effect is controlled by the control unit introduced in §IV-D. A current sensing module (Adafruit ina219 breakout) is connected in series with the electric load in the circuit to measure the high-side current and voltage to calculate the power of regeneration in real-time. A potentiometer (ALPS RDC503) is used to measure the joint angle. The velocity is then estimated by finite differences on the position data. The software architecture is based on the open-source Robot Operating System (ROS), where the

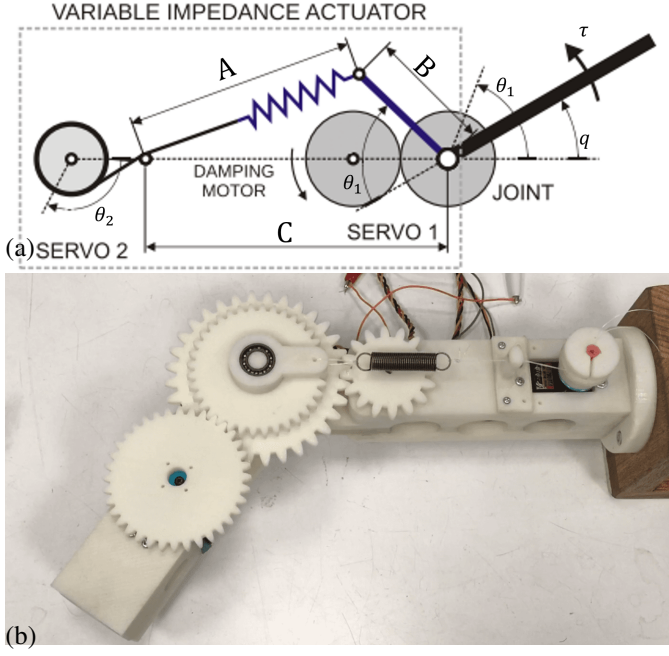


Fig. 7: (a) Schematic diagram and (b) hardware of Mechanically Adjustable Compliance and Controllable Equilibrium Position Actuator [33] with variable damping [7]. In the results reported here, $B = 3.6$ cm, $C = 13.5$ cm, $r = 1.5$ cm and the spring has linear spring constant $\kappa = 394$ N/m. The link has inertia $m = 0.0036$ kgm² and friction coefficient $b = 0.0077$ Nms/rad. The gear ratio between the joint and damping motor is $n_d = 40$.

control command is published to a ROS message, which is then subscribed by a microcontroller (Arduino mega2560) to control the servomotors and the damping unit.

B. Control of the variable impedance robot

The variable impedance mechanism has intrinsic redundancy in its internal actuation. Optimal control has been demonstrated to be a straightforward and simple way to resolve this redundancy [34] and efficient numerical solutions are available through local, iterative algorithms, such as ILQR. In the experiments reported here, ILQR is used to design the control sequence for the robot on the fly, as each reaching target is generated.

1) *Robot dynamics*: To determine the optimal control sequence, ILQR requires a model of the dynamics of the system. For the MACCEPA-VD, the dynamics are governed by the equations

$$\ddot{q} = (\tau_s - d(u_3)\dot{q} - b\dot{q} - \tau_{\text{ext}})m^{-1} \quad (20)$$

$$\ddot{\theta}_1 = \beta^2(u_1 - \theta_1) - 2\beta\dot{\theta}_1 \quad (21)$$

$$\ddot{\theta}_2 = \beta^2(u_2 - \theta_2) - 2\beta\dot{\theta}_2 \quad (22)$$

where q, \dot{q}, \ddot{q} are the joint angle, velocity and acceleration, respectively, b is the viscous friction coefficient for the joint, m is the link inertia, τ_s is the torque generated by the spring force, and τ_{ext} is the joint torque due to external loading (the following reports results for the case of no external loading, i.e., $\tau_{\text{ext}} = 0$). $\theta_1, \theta_2, \dot{\theta}_1, \dot{\theta}_2, \ddot{\theta}_1, \ddot{\theta}_2$ are the motor angles, velocities and accelerations. The motor angles θ_1, θ_2

are controlled by $u_1 \in [-\pi/3, \pi/3]$, $u_2 \in [0, \pi/3]$ respectively. The servomotor dynamics (21), (22) are assumed to behave as a critically damped system,⁶ with $\beta = 25$.

The torque τ_s can be calculated as follows:

$$\tau_s = \kappa BC \sin(\theta_1 - q) \left(1 + \frac{r\theta_2 - |C - B|}{A(q, \theta_1)}\right) \quad (23)$$

where $A(q, \theta_1) = \sqrt{B^2 + C^2 - 2BC \cos(\theta_1 - q)}$, B and C are the lengths shown in Fig. 7, r is the radius of the winding drum used to adjust the spring pre-tension, and κ is the linear spring constant. The damping coefficient $d(u_3)$ depends on control input u_3 and is calculated according to the damping scheme used (i.e., (2), (3) or (8)). Note also that, the stiffness of this system depends on the joint and motor positions q, θ_1, θ_2

$$k(q, \theta_1, \theta_2) = \kappa BC \cos(\theta_1 - q) \left(1 + \frac{r\theta_2 - |C - B|}{A}\right) - \frac{\kappa B^2 C^2 \sin^2(\theta_1 - q(r\theta_2 - |C - B|))}{A^{\frac{3}{2}}}. \quad (24)$$

2) *Optimal control formulation*: To represent the problem as an optimal control problem the dynamics are formulated as a state-space model $\dot{\mathbf{x}} = \mathbf{f}(\mathbf{x}, \mathbf{u})$, where $\mathbf{x} = (x_1, x_2, x_3, x_4, x_5, x_6)^T = (q, \dot{q}, \theta_1, \theta_2, \dot{\theta}_1, \dot{\theta}_2)^T \in \mathbb{R}^6$ denotes the state space vector, $\mathbf{u} = (u_1, u_2, u_3)^T \in \mathbb{R}^3$ is the control input, and \mathbf{f} is defined as

$$\mathbf{f} = \begin{cases} x_2 \\ (\tau_s(x_1, x_2, x_3) - (d(u_3) + b)x_2)m^{-1} \\ x_5 \\ x_6 \\ \beta^2(u_1 - x_3) - 2\beta x_5 \\ \beta^2(u_2 - x_4) - 2\beta x_6 \end{cases} \quad (25)$$

The task of point-to-point reaching is captured by the cost function

$$J = \int_0^{t_f} (w_1(q - q^*)^2 + w_2 F_s^2 + w_3(u_3 - 0.5)^2 + w_4 \mathbf{u}^T \mathbf{u}) dt \quad (26)$$

where q^* is the reaching target, F_s is the spring force, and t_f is the reaching duration (for simplicity, in the experiments reported below, this is fixed at $t_f = 1.5$ s for each movement). Here, the first term represents the reaching error and has weight $w_1 = 1000$ and the second term penalises the squared spring force ($w_2 = 1$) which accounts for minimising energy consumption.⁷ The third term penalises deviation of damping control from 0.5 (since this is known to be the point at which the regeneration coefficient is maximised, see §IV) to encourage energy regeneration (in the experiments reported here it is weighted at $w_3 = 500$). The last term is added for regularisation of the optimal control solution ($w_4 = 10^{-6}$). Note that, it is possible to use predicted regeneration power to replace the third term, however, it may result in behaviours

⁶This 2nd order dynamical model is widely used in the literature, e.g., in [34]. Here, the coefficient β is chosen empirically to fit the step response of the servomotors.

⁷An full model of the energy consumption of this actuator is not available. However, due to its mechanical design (with the spring pre-tension motor working against the spring), the overall electrical power consumption is monotonically related to squared spring force.

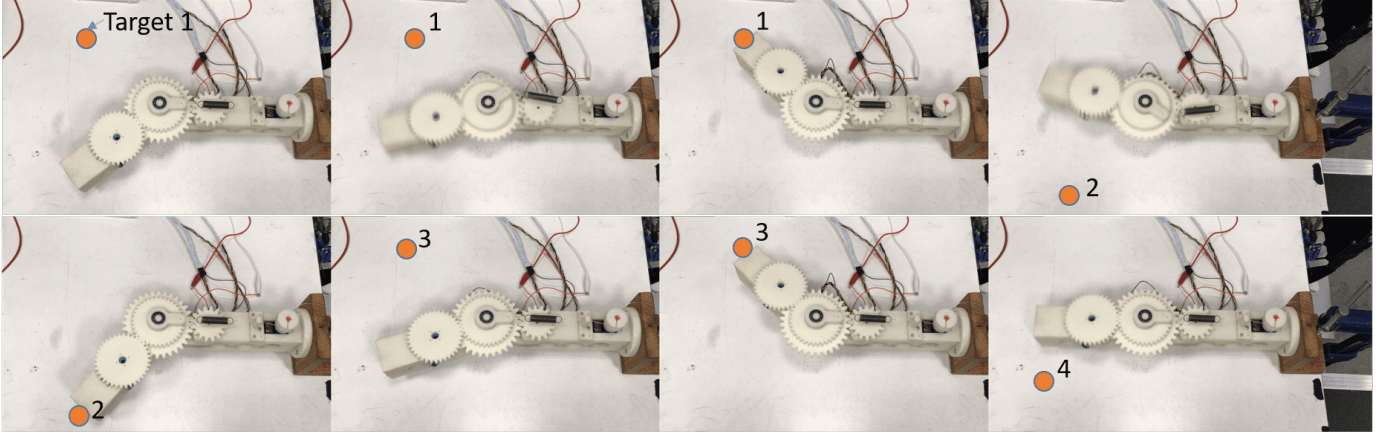


Fig. 8: Snapshots of consecutive point-to-point reaching in the VSVD condition. The orange points overlaid show the reaching targets.

sensitive to modelling errors of both dynamics and power regeneration.

C. Consecutive point-to-point reaching experiment

The task chosen to evaluate the proposed scheme is consecutive point-to-point reaching to random targets. The experimental procedure is as follows.

A list of $N = 25$ locations are generated sequentially as targets for reaching. Each target is drawn uniform randomly (i.e., $q^* \sim U[-\pi/3, \pi/3]$), with the minimal distance between the target and the preceding one restricted to be at least $\pi/3$, to exclude very short-range movements. After generation, each target is fed to the cost function (26), and ILQR is used to determine the optimal control sequence for the movement under the dynamics (25), utilising the whole control input space (i.e., where all three control variables u_1 , u_2 and u_3 are exploited to seek the optimum). The solutions are then executed on the plant, and the resultant joint trajectories and regenerated current are recorded. This procedure is repeated $M = 20$ times to get a total of 500 recorded trajectories for performance evaluation. (In the below, this is termed the *variable stiffness variable damping* (VSVD) condition.) Fig. 8 shows snapshots of reaching movements made to a typical sequence of targets.

For comparison, using the same reaching targets, the above procedure is repeated under three further conditions, namely (i) *fixed stiffness and fixed damping* (FSFD): a baseline set where u_1 , u_2 and u_3 are held at to constant values (in this case, reaching occurs by setting $u_1 = q^*$ prior to the onset of each reaching movement), (ii) *fixed stiffness and variable damping* (FSVD): only the damping control u_3 is optimised, while u_1 and u_2 are held at fixed values, (iii) *variable stiffness and fixed damping* (VSFD): the damping command u_3 is fixed and the equilibrium position and stiffness control inputs are optimised. In the conditions where the stiffness is fixed (i.e., FSFD and FSVD), u_2 is set to the minimal stiffness motor angle⁸ $\pi/6$. In the conditions where the damping is fixed (i.e., FSFD and VSFD), the damping command is set at $u_3 = 0.5$, corresponding to the point at which the regeneration coefficient reaches its maximum.

⁸The minimal stiffness motor angle is selected empirically to add sufficient pretension of the spring to provide good reaching accuracy around the zero joint position.

D. Performance metrics

In order to quantitatively compare the results, four metrics are employed to take into account of movement performance as well as energy consumption and regeneration:

Settling time The time when the plant settles down. For a given trajectory, this is defined as the smallest time t where both velocity and acceleration are within the vicinity of zero, i.e., $|\dot{q}_t| < \epsilon_1$ and $|\ddot{q}_t| < \epsilon_2$. In our experiments, ϵ_1 was chosen to be approximately 1% of the maximum measured velocity and ϵ_2 was chosen to be 1.5% of maximum measured acceleration.

Overshoot The deviation of the joint position from the target point after over-shooting the target. It is defined as the integration of $(q_t - q^*)^2$ from the time at which the target is first reached until the plant settles.

Energy consumption E_{in} computed by integrating P_{in} (defined in §II-A).

Regenerated energy E_{rege} computed by integrating the measured regeneration power.

Each of these are computed using the experimentally recorded data from the robot. For each trial, the settling time and overshoot of N trajectories are averaged and the energy regeneration and consumption are accumulated.

E. Results

The results for the four experimental conditions are reported in TABLE I and their scores are visualised in the radar chart⁹ in Fig. 9. Looking at each of these, it can be seen that in all conditions the damping module successfully regenerates power during the movement (see, for example, Fig. 10(c) where a monotonic increase in accumulated energy is seen). Note, however, there is a discrepancy in the amount of energy regenerated and the corresponding performance in the reaching task.

As seen in Fig. 9, the baseline condition (FSFD) harvests the most energy, by fixing the damping to the value that provides maximum regeneration coefficient. Although this simple

⁹In the radar chart, the higher the score one gets in a dimension, the better the performance against its corresponding metric. For example, the energy regeneration score, denoted by γ_r , is the value of E_{rege} normalised according to its maximum and minimum values in the four experimental conditions. $\gamma_t, \gamma_o, \gamma_c$, which refer to the normalised settling time, overshoot and energy consumption, respectively, are computed similarly.

Experiment	Settling time (s)	Overshoot ($10^{-2}\text{rad}^2\text{s}$)	E_{in} (J)	E_{rege} (J)
FSFD	1.064 ± 0.039	4.980 ± 1.040	4.080 ± 0.552	0.152 ± 0.019
FSVD	0.923 ± 0.063	1.050 ± 0.350	3.989 ± 0.541	0.071 ± 0.014
VSFD	0.792 ± 0.061	0.650 ± 1.990	3.412 ± 0.358	0.089 ± 0.006
VSVD	0.780 ± 0.045	0.270 ± 0.120	3.067 ± 0.338	0.092 ± 0.010

TABLE I: Performance metrics for the four experimental conditions computed on the recorded reaching data. Shown are mean \pm standard deviation of each metric over 20 trials.

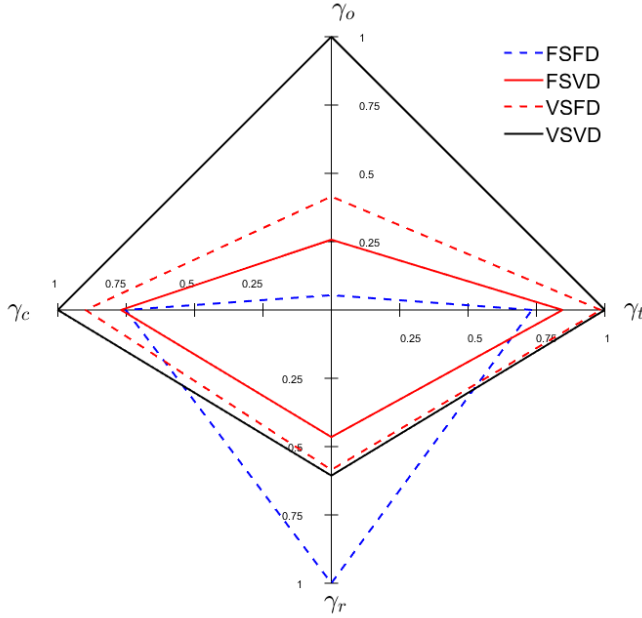


Fig. 9: Radar chart showing the normalised reaching scores under the four experimental conditions. The higher the score the better the performance. Shown are mean scores over 20 trials.

control strategy results in the most energy regeneration in the experiments, it sacrifices movement performance, scoring lowest in terms of the overshoot and settling time. Looking at the trajectory in Fig. 10 (dashed blue line), it can be seen that there is significant overshoot for multiple targets. The enhanced energy regeneration also does not translate to lower energy consumption (see Fig. 9 and TABLE I). All this suggests that, although the stiffness and damping can be pre-tuned to give good performance for a specific movement, it can only be a solution for a specific task, and thus not suitable for a versatile actuator.

With FSVD, the movement performance in terms of overshoot and settling time is improved compared to FSFD, although the decrease in energy consumption is insignificant. The result confirms that variable damping can be utilised to improve the dynamic performance when the joint has fixed stiffness profile. It gives good overall dynamic performance for varied reaching targets. However, without exploiting variable stiffness, the variable damping cannot ensure energy efficient movements alone. In Fig. 9 it can be seen that FSVD regenerates the least energy and there is no obvious improvement in terms of energy consumption.

By modulating the equilibrium position and stiffness VSFD performs moderately better on all performance metrics compared to FSVD. However, when all impedance variables are

available to the controller, as in condition VSVD, it can be seen that the performance is significantly improved across the different metrics compared to the other conditions (see Fig. 9). The energy efficiency is improved because there is less consumption (E_{in}) and more regeneration (E_{rege}). Additionally, although the average settling time is almost the same as that of VSFD, there is significantly lower overshoot.

Overall, these comparisons show that using variable damping in combination with an optimally exploited variable stiffness mechanism can contribute both enhanced dynamic performance and improved energy efficiency (in terms of both consumption and regeneration).

F. Loss of regeneration through over-exploitation of damping

Comparing the performance of FSFD and FSVD it can be seen that a relatively modest improvement in reaching performance comes at the cost of a large reduction in the energy regeneration level. This seems surprising since FSVD also has available the possible strategy of keeping the damping fixed (although the damping can be varied, there is no imperative to do so). To better understand this behaviour, it is illuminating to examine in detail the control strategies chosen under the different conditions.

To examine this issue, the trajectories for reaching to a typical target position under the experimental conditions FSVD, VSFD and VSVD is plotted in Fig. 11. Looking at Fig. 11(a), the accuracy is relatively good for each of the conditions (with some small overshoot in the FSVD condition). However, to achieve this accuracy, the FSVD controller, being unable to modulate speed by any other means, modulates the damping over its full range, maintaining a high damping constant during braking ($0.2 < t < 0.5$ s), see Fig. 11(d). As the rate of energy regeneration has its maximum at $u_3 = 0.5$, the more time the damping is held away from its medium value, the lower the total accumulated energy will be (see §IV). In contrast, the damping command of VSVD remains low during the acceleration phase to decrease the loss and required input power, but then maintains the damping command close to the maximum regeneration damping level for the remainder of the movement. This is thanks to its ability to modulate the joint stiffness and thereby effect braking by an alternative means (see Fig. 11(b) and Fig. 11(c)). The variable stiffness therefore provides some flexibility in control to prevent the *over-exploitation of variable damping* and the associated loss of regeneration.

VII. CONCLUSIONS

This paper proposes an extension to variable damping module design for VIAs based on the motor braking effect. In contrast to previous, pure dynamic braking designs, the proposed approach provides a solution for realising controllable damping, which enables the VIAs to regenerate dissipated energy from

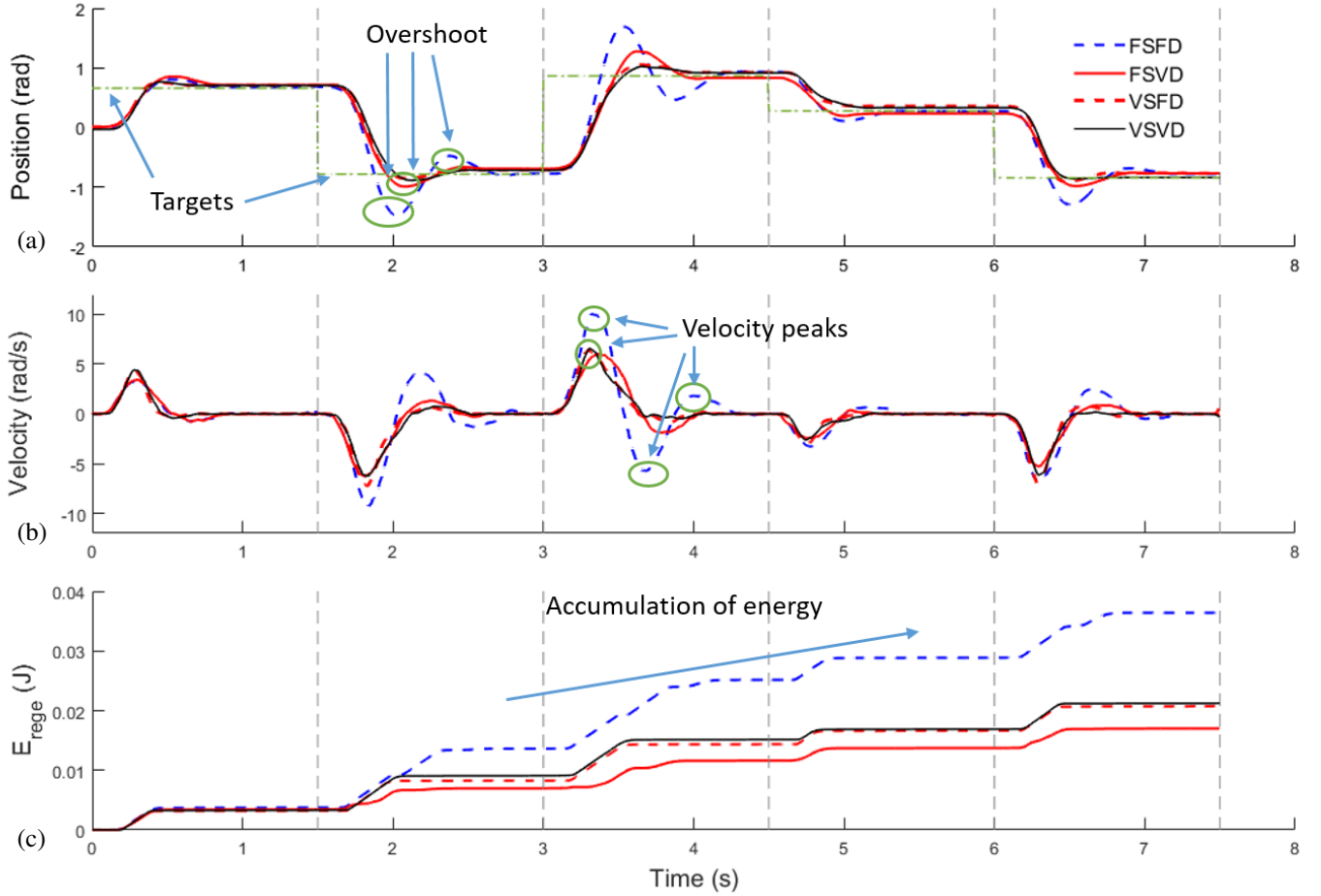


Fig. 10: Recorded trajectories (a) joint position, (b) velocity, and (c) accumulation of regenerated energy E_{rege} of five typical examples of consecutive point-to-point reaching movements. The end of each movement is represented by the vertical dashed line. The dot-dashed line in (a) shows the target position for each phase of movement.

bidirectional movement to charge a unidirectional electric storage element. Furthermore, it overcomes the drawback of a reduction in the maximum damping effect found in pure regenerative braking schemes.

The control input for this damping module simply varies from 0 to 1, representing a proportional percentage of the maximum damping. As the power regeneration has a non-monotonic relation with the control input and damping coefficient (as verified by experiment), the balancing between damping allocation and energy regeneration needs to be treated with care. However, application of the hybrid damping module to VIAs verified by experiments, shows that the actuation redundancy is solved by optimal control successfully to achieve fast smooth movement while still enabling power regeneration.

To investigate the use of variable regenerative damping for long-term operation, a stochastic consecutive reaching task was designed to examine the movement performance and energy efficiency. The experimental study shows that exploiting exploiting variable stiffness and variable damping is desired, in such a way that there is more flexibility to prevent over-exploitation of variable damping and loss of regeneration capability.

In future work, further prototyping of the power electronics and mechanical elements will be investigated to improve the transmission efficiency of the regenerative damping system.

Furthermore, it is planned to investigate the use of the damping module for more complex long-term behaviours such as long-distance locomotion using a bipedal platform. Model learning techniques will be employed to produce accurate prediction of energy cost and regeneration for optimisation towards long-term energy efficiency. Such information can be potentially used for high-level planning and human-guided learning control.

REFERENCES

- [1] Paryanto, M. Brossog, M. Bornschlegel, and J. Franke, "Reducing the energy consumption of industrial robots in manufacturing systems," *International Journal of Advanced Manufacturing Technology*, vol. 78, no. 5-8, pp. 1315-1328, 2015.
- [2] B. Vanderborght, A. Albu-Schaeffer, A. Bicchi, E. Burdet, D. Caldwell, R. Carloni, M. Catalano, G. Ganesh, M. Garabini, M. Grebenstein, G. Grioli, S. Haddadin, A. Jafari, M. Laffranchi, D. Lefeber, F. Petit, S. Stramigioli, N. Tsagarakis, M. Van Damme, R. Van Ham, L. C. Visser, and S. Wolf, "Variable impedance actuators: Moving the robots of tomorrow," in *IEEE Int. Conf. Intelligent Robots & Systems*, 2012.
- [3] M. Grebenstein, A. Albu-Schaeffer, T. Bahls, M. Chalon, O. Eiberger, W. Friedl, R. Gruber, S. Haddadin, U. Hagn, R. Haslinger, H. Hoppner, S. Jorg, M. Nickl, A. Nothhelfer, F. Petit, J. Reill, N. Seitz, T. Wimbock, S. Wolf, T. Wusthoff, and G. Hirzinger, "The DLR hand arm system," in *IEEE Int. Conf. Robotics & Automation*, 2011.
- [4] B. Vanderborght, A. Albu-Schaeffer, A. Bicchi, A. Albu-Schaeffer, A. Bicchi, E. Burdet, D. Caldwell, R. Carloni, M. Catalano, O. Eiberger, W. Friedl, G. Ganesh, M. Garabini, M. Grebenstein, G. Grioli, S. Haddadin, H. Hoppner, A. Jafari, M. Laffranchi, D. Lefeber, F. Petit,

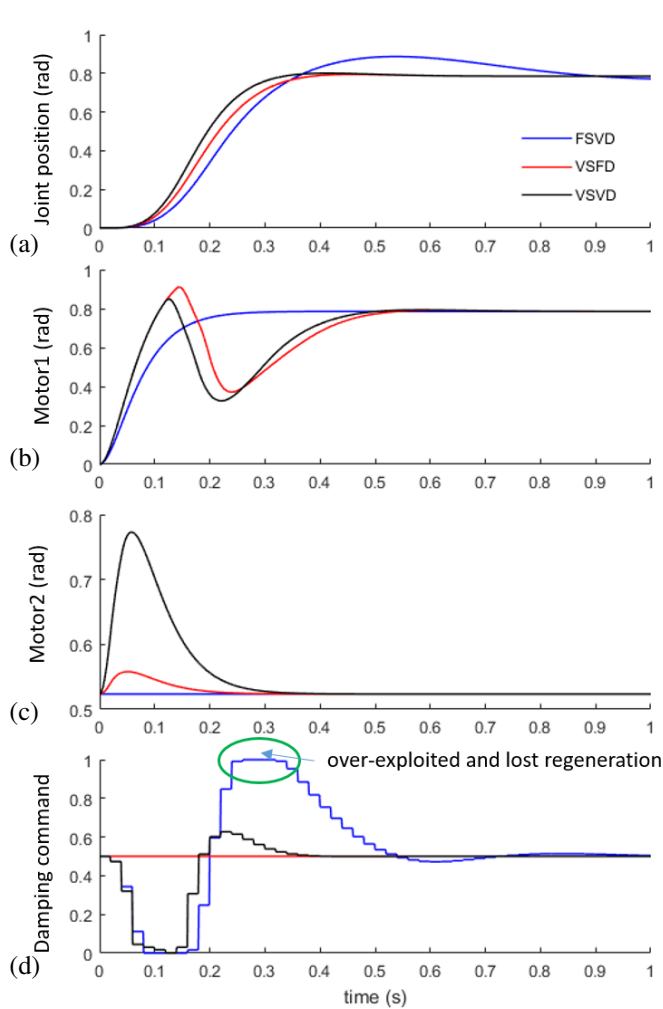


Fig. 11: Comparison of a single reaching movement to the same target position under the conditions FSVD, VSFD and VSVD. The figure shows the (a) joint position, (b) motor 1, (c) motor 2, and (d) damping command against time.

S. Stramigioli, N. Tsagarakis, M. Van Damme, R. Van Ham, L. Visser, and S. Wolf, "Variable impedance actuators: A review," in *IEEE Int. Conf. Intelligent Robots & Systems*, 2013.

[5] M. Laffranchi, L. Chen, N. G. Tsagarakis, and D. G. Caldwell, "The role of physical damping in compliant actuation systems," in *IEEE Int. Conf. Intelligent Robots & Systems*, 2012.

[6] M. Laffranchi, N. G. Tsagarakis, and D. G. Caldwell, "CompAct Arm: a Compliant Manipulator with Intrinsic Variable Physical Damping," in *Robotics: Science and Systems VIII*, 2013.

[7] A. Radulescu, M. Howard, D. J. Braun, and S. Vijayakumar, "Exploiting variable physical damping in rapid movement tasks," in *IEEE/ASME Int. Conf. Advanced Intelligent Mechatronics*, 2012.

[8] F. Wu and M. Howard, "A Hybrid Dynamic-Regenerative Damping Scheme for Energy Regeneration in Variable Impedance Actuators," in *IEEE Int. Conf. Robotics & Automation*, IEEE, 2018, pp. 4277–4282.

[9] S. H. Collins, A. Ruina, R. Tedrake, and M. Wisse, "Efficient Bipedal Robots Based on Passive-Dynamic Walkers," *Science*, vol. 307, no. 5712, pp. 1082–1085, 2005.

[10] R. E. Hellmund, "Regenerative Braking of Electric Vehicles," *Transactions of the American Institute of Electrical Engineers*, vol. XXXVI, pp. 1–78, 1917.

[11] R. Zhang, X. Wang, and S. John, "A comprehensive review of the techniques on regenerative shock absorber systems," *Energies*, vol. 11, no. 5, 2018.

[12] J. M. Donelan, Q. Li, V. Naing, J. A. Hoffer, D. J. Weber, and A. D. Kuo, "Biomechanical energy harvesting: Generating electricity during walking with minimal user effort," *Science*, vol. 319, no. 5864, pp. 807–810, 2008.

[13] S. H. Collins and A. Ruina, "A bipedal walking robot with efficient and human-like gait," in *IEEE Int. Conf. Robotics & Automation*, 2005.

[14] B. Vanderborght, B. Verrelst, R. Van Ham, M. Van Damme, D. Lefeber, B. M. Y. Duran, and P. Beyl, "Exploiting Natural Dynamics to Reduce Energy Consumption by Controlling the Compliance of Soft Actuators," *The International Journal of Robotics Research*, vol. 25, no. 4, pp. 343–358, 2006.

[15] B. VanderBorgh, B. Verrelst, R. Van Ham, M. Van Damme, P. Beyl, and D. Lefeber, "Development of a compliance controller to reduce energy consumption for bipedal robots," *Autonom. Robots*, vol. 24, no. 4, pp. 419–434, 2008.

[16] M. Hutter, C. D. Remy, M. a. Hoepflinger, and R. Siegwart, "Efficient and Versatile Locomotion With Highly Compliant Legs," *IEEE/ASME Transactions on Mechatronics*, vol. 18, no. 2, pp. 449–458, 2013.

[17] S. K. Au, J. Weber, and H. Herr, "Biomechanical Design of a Powered Ankle-Foot Prosthesis," in *IEEE 10th International Conference on Rehabilitation Robotics*, 2007, pp. 298–303.

[18] S. Haddadin, K. Krieger, M. Kunze, and A. Albu-sch, "Exploiting potential energy storage for cyclic manipulation: An analysis for elastic dribbling with an anthropomorphic robot," in *IEEE/RSJ International Conference on Intelligent Robots and Systems*, 2011.

[19] D. Lakatos, F. Petit, and A. Albu-Schffer, "Nonlinear oscillations for cyclic movements in human and robotic arms," *IEEE Transactions on Robotics*, vol. 30, no. 4, pp. 865–879, Aug 2014.

[20] A. Velasco, M. Garabini, M. G. Catalano, and A. Bicchi, "Soft actuation in cyclic motions: Stiffness profile optimization for energy efficiency," in *IEEE-RAS 15th International Conference on Humanoid Robots (Humanoids)*, 2015, pp. 107–113.

[21] K. Matsusaka, M. Uemura, and S. Kawamura, "Realization of highly energy efficient pick-and-place tasks using resonance-based robot motion control," *Advanced Robotics*, vol. 30, no. 9, pp. 608–620, 2016.

[22] S. Haddadin, K. Krieger, A. Albu-Schaffer, and T. Lilge, "Exploiting elastic energy storage for blind cyclic manipulation: Modeling, stability analysis, control, and experiments for dribbling," *IEEE Transactions on Robotics*, vol. 34, no. 1, pp. 91–112, 2018.

[23] D. Braun, M. Howard, and S. Vijayakumar, "Optimal variable stiffness control: formulation and application to explosive movement tasks," *Autonomous Robots*, vol. 33, no. 3, pp. 237–253, 2012.

[24] M. C. Ozparpucu and S. Haddadin, "Optimal control for maximizing link velocity of visco-elastic joints," in *2013 IEEE/RSJ International Conference on Intelligent Robots and Systems*, 2013, pp. 3035–3042.

[25] M. H. Raibert, *Legged Robots That Balance*. Cambridge, MA, USA: Massachusetts Institute of Technology, 1986.

[26] J. Nakanishi, K. Rawlik, and S. Vijayakumar, "Stiffness and temporal optimization in periodic movements: An optimal control approach," in *IEEE/RSJ International Conference on Intelligent Robots and Systems*, no. 1, 2011, pp. 718–724.

[27] A. Jafari, N. Tsagarakis, and D. Caldwell, "Energy efficient actuators with adjustable stiffness: a review on awas, awas-ii and compact vsa changing stiffness based on lever mechanism," *Industrial Robot: An International Journal*, vol. 42, no. 3, pp. 242–251, 2015.

[28] D. J. Braun, S. Apte, O. Adiyatov, A. Dahiya, and N. Hogan, "Compliant actuation for energy efficient impedance modulation," in *IEEE International Conference on Robotics and Automation*, 2016, pp. 636–641.

[29] M. Plooi, M. Wisse, and H. Vallery, "Reducing the energy consumption of robots using the bidirectional clutched parallel elastic actuator," *IEEE Transactions on Robotics*, vol. 32, no. 6, pp. 1512–1523, 2016.

[30] R. Jimenez-Fabian, J. Geeroms, L. Flynn, B. Vanderborght, and D. Lefeber, "Reduction of the torque requirements of an active ankle prosthesis using a parallel spring," *Robotics and Autonomous Systems*, vol. 92, pp. 187 – 196, 2017.

[31] S. Seok, A. Wang, M. Y. M. Chuah, D. J. Hyun, J. Lee, D. M. Otten, J. H. Lang, and S. Kim, "Design principles for energy-efficient legged locomotion and implementation on the mit cheetah robot," *IEEE/ASME Transactions on Mechatronics*, vol. 20, no. 3, pp. 1117–1129, 2015.

[32] W. Li and E. Todorov, "Iterative Linear Quadratic Regulator Design for Nonlinear Biological Movement Systems," in *IEEE Int. Conf. Robotics & Automation*, 2004.

[33] R. Van Ham, B. Vanderborght, M. Van Damme, B. Verrelst, and D. Lefeber, "MACCEPA, the mechanically adjustable compliance and controllable equilibrium position actuator: Design and implementation in a biped robot," *Rob. Auton. Syst.*, vol. 55, no. 10, pp. 761–768, 2007.

[34] D. Braun, F. Petit, F. Huber, S. Haddadin, P. Van Der Smagt, A. Albu-Schaffer, and S. Vijayakumar, "Robots driven by compliant actuators: Optimal control under actuation constraints," *IEEE Transactions on Robotics*, vol. 29, no. 5, pp. 1085–1101, 2013.